Journal of Alloys and Compounds, 187 (1992) 157–169
JALCOM 300

Polarization dependent X-ray absorption study of Cu_xNbS_2 ($x=0.00$, 0.16) and Cu_xNbSe_2 ($x=0.00$, 0.38)*

J. Freund and G. Wortmann
Fachbereich Physik, Universität-GH-Paderborn, 4790 Paderborn (Germany)

W. Paulus
Laboratoire Léon Brillouin, CEN Saclay, 91191 Gif-sur-Yvette, Cédex (France)

W. Krone
Fachbereich Physik, Freie Universität Berlin, 1000 Berlin 33 (Germany)

(Received March 11, 1992)

Abstract

The X-ray absorption fine structure (XAFS) of single crystals of NbS_2, $Cu_{0.16}NbS_2$, $NbSe_2$ and $Cu_{0.38}NbSe_2$ is investigated at the Nb, Se and Cu edges. Measurements are made for different angles between the crystallographic c-axis and the X-ray beam. Nearest-neighbor and next-nearest-neighbor distances, as well as their variances, are extracted from the extended XAFS (EXAFS), indicating that intercalation of copper does not affect the average distances within the Nb–chalcogen layers while, at the same time, a structural disorder is introduced. The X-ray absorption near edge structure (XANES) of Cu_xNbSe_2 is sensitive to the direction of empty electronic states and indicates that empty states with z-symmetry are separated from empty states with x- and y-symmetry by about 2.5 eV. It also shows that intercalation is accompanied by charge transfer from the Cu to the $NbSe_2$ host lattice.

1. Introduction

The transition metal dichalcogenides NbS_2 and $NbSe_2$ are layer compounds consisting of sandwiches with strong covalent/ionic intralayer bonds and weak Van der Waals interlayer interactions. Monovalent transition metals, such as Cu or Ag, can be inserted between the sandwiches. One sandwich consists of two hexagonal close packed layers of S or Se atoms, forming trigonal prisms filled with Nb atoms (Fig. 1). The stacking sequences of S (upper case letters) and Nb (lower case letters) are AcA BcB (2H–NbS_2 structure) or AbA BcB CaC (3R–MoS_2 structure) [1, 2]. For $NbSe_2$ several more stacking sequences exist [1, 3]. Upon sufficient intercalation of Cu the stacking sequences change [2, 4]. The intercalated Cu atoms occupy tetrahedral or octahedral sites either in a random fashion or by forming superstructures, depending on the temperature and on the concentration of Cu [5–7].

*Contribution to the Conference on Solid Compounds of Transition Elements, Münster, May 21–25, 1991.

0925-8388/92/$5.00

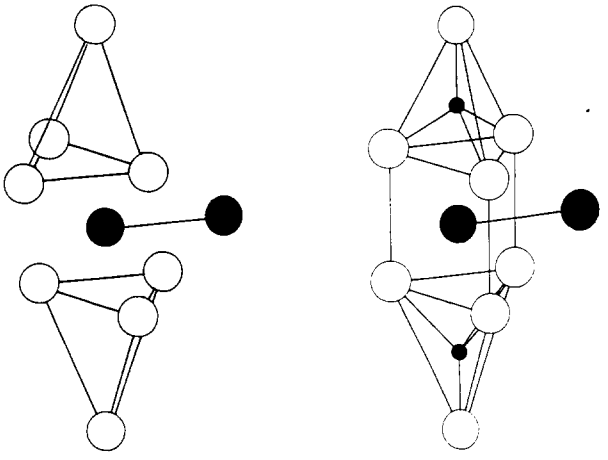

Fig. 1. Schematic drawing of the crystal structure of Cu_xNbS_2 and Cu_xNbSe_2 showing nearest and next-nearest-neighbor coordinations. Open circles represent S or Se atoms, large (small) black circles represent Nb (Cu) atoms [16].

A number of X-ray absorption near-edge structure (XANES) and extended X-ray absorption fine structure (EXAFS), together referred to as X-ray absorption fine structure (XAFS), experiments have been made with NbS_2, $NbSe_2$ and their intercalated variants [8–15]. Our experiments, reported in this paper, were made in transmission geometry at 80 and 300 K by measuring the absorption of polarized synchrotron radiation by single crystals of NbS_2, $Cu_{0.16}NbS_2$, $NbSe_2$ and $Cu_{0.38}NbSe_2$ and tilting the crystals so as to "focus" on different directions. Our main attention was on $Cu_{0.38}NbSe_2$, where measurements were made at all three edges.

After a section on experimentation and data analysis, we present quantitative and some qualitative nearest-neighbor and next-nearest-neighbor structural results from the EXAFS part of the spectra and make comparisons with results obtained from single crystal X-ray diffraction experiments on $Cu_{0.38}NbSe_2$ [16]. Finally, we present some results on intercalation-induced changes of the electronic structure determined from the XANES part of the spectra and discuss these findings with respect to the charge transfer in Cu_xNbSe_2.

2. Experimentation and data analysis

The samples of NbS_2, $Cu_{0.16}NbS_2$, $NbSe_2$ and $Cu_{0.38}NbSe_2$ were prepared by chemical vapor transportation in evacuated and sealed quartz ampoules at elevated temperatures. We started from the pure elements (Nb 99.8%, S 99.98%, Se 99.98%, Cu 99.99%) with iodine used as carrier. The temperature gradient in the two zone furnaces was 970 °C → 940 °C for the sulfides and 850 °C → 750 °C for the selenides. Stoichiometric amounts were used for

$Cu_{0.38}NbSe_2$ while the sulfides were transported under sufficiently high sulfur pressure with a Nb/S ratio of 1/2.5 in order to avoid excess Nb between the NbS_2 slabs. After two weeks the samples were quenched in an ice–water mixture.

The single crystals thus produced were inserted into the X-ray beam of the RÖMO II beamline of HASYLAB at DESY (Hamburg). A double crystal Si(311) monochromator was used, and contamination with higher harmonics was suppressed by detuning the monochromator. Absorption spectra were taken in transmission at the K edges of Nb, Se and Cu at temperatures of 80 and 300 K and for several tilt angles between the direction of the beam and the c-axes of the single crystals. In addition to the K edges of the materials mentioned above, the K edge spectra of pure Nb, Cu and Se were measured simultaneously in order to obtain relative energy references.

In the usual way [17], EXAFS data analysis comprises post-edge background removal with a cubic spline and normalization of the spectrum by division through the step height to produce the EXAFS interference function, $\chi(k)$. The interference function is weighted with k^x (Fig. 2), with x being 1 (Se edge in Cu_xNbSe_2), 2 (Cu edge in $Cu_{0.16}NbS_2$, and Nb edge in Cu_xNbSe_2) or 3 (Nb edge in Cu_xNbS_2), multiplied by a gaussian window extending from about 2 to 15–16 $Å^{-1}$ (Nb edge), 2–16 $Å^{-1}$ (Se edge) or 2–8 $Å^{-1}$ (Cu edge), and subjected to a Fourier transform from k-space to r-space (Figs. 3–5). The r-space data are then subjected to a Fourier back-transform after application of a gaussian window covering the first or second nearest-neighbor shell respectively.

The single-shell data thus produced are fitted to the single scattering EXAFS formula including cumulants up to second order (harmonic approximation),

$$\chi(k) = A(k)\,\sin[\Psi(k)] \tag{1}$$

with the amplitude

$$A(k) = \left[\sum_{j=1}^{N} 3(\hat{\epsilon}\cdot\hat{\boldsymbol{R}}_j)^2\right] \frac{F(k,\pi)f}{kR^2} \exp(-2R/\lambda(k)) \exp(-2\sigma^2k^2) \tag{2}$$

and the phase

$$\Psi(k) = 2k\left[R - \frac{2\sigma^2}{R}\left(1 + \frac{R}{\lambda(k)}\right)\right] + \Phi(k) \tag{3}$$

where N is the coordination number, $\hat{\epsilon}$ the direction of the X-ray polarization (*i.e.* the direction of the $\boldsymbol{E}$-field), $\hat{\boldsymbol{R}}_j$ the unit vector to the jth backscattering atom, $F(k, \pi)$ the back-scatter amplitude, f an amplitude correction factor, R the distance to the shell, $\lambda(k)$ the electron mean free path, σ^2 the second cumulant, *i.e.* the variance of the distance from the absorbing atom to the shell under consideration, and $\Phi(k)$ the combined central atom and backscatter phase shift. k is the electron wave-vector which depends on ΔE, the shift between the assumed and the real zero of the free electron states. While the products $\hat{\epsilon}\cdot\hat{\boldsymbol{R}}_j$ are known for a given structure, $F(k, \pi)$, $\lambda(k)$ and $\Phi(k)$

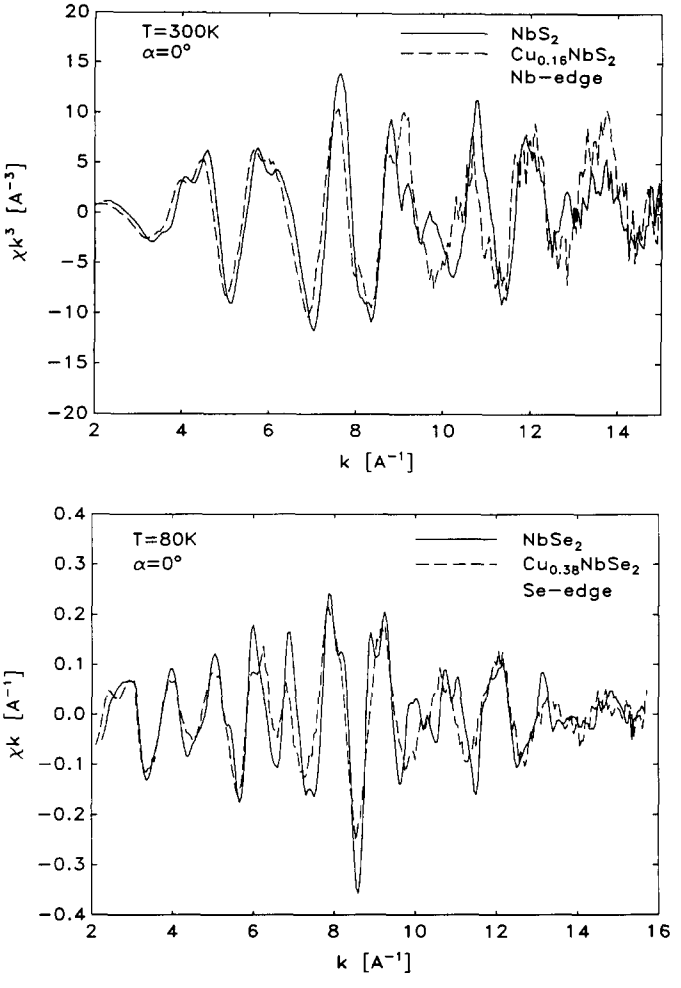

Fig. 2. EXAFS interference function $\chi(k)$ of Cu_xNbS_2 and Cu_xNbSe_2 weighted with k^3 and k respectively. α is the angle between the X-ray beam and the crystallographic c-axis.

are taken from the FEFF calculations (version 3.23) of Rehr *et al.* [18, 19]. This leaves f, R, σ^2 and ΔE as fit parameters.

Equation (2) shows that absorption by a single crystal (with well-defined directions to back-scattering atoms $\hat{\boldsymbol{R}}_j$) of synchrotron radiation (with a well-defined $\hat{\epsilon}$ in the plain of the storage ring and at right angles to the direction of the X-ray beam) is sensitive to the position of the crystal in the beam. Thus, by tilting the crystal, information from different directions of the crystal can be emphasized as long as the symmetry is lower than cubic. Layered systems, such as the present ones or graphite intercalation compounds [20], are therefore particularly suitable for angle-sensitive investigations. When a polycrystalline material is used, the summation over N distinct directions is replaced by N integrations over the sphere,

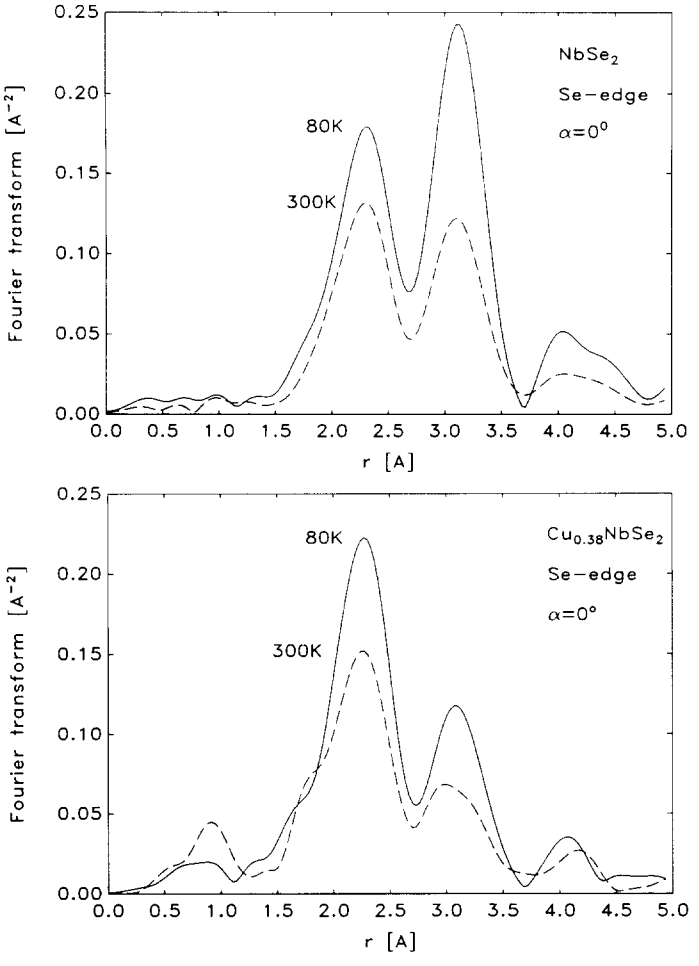

Fig. 3. Fourier forward transforms of Cu_xNbSe_2 (Se edge) as a function of temperature when the crystallographic c-axis is parallel to the X-ray beam ($\alpha=0$).

$$\sum_{j=i}^{N} 3(\hat{\epsilon}\cdot\hat{\boldsymbol{R}}_j)^2 \longrightarrow N\frac{\int_{4\pi} 3\cos^2\Theta\,\mathrm{d}\Omega}{\int_{4\pi}\mathrm{d}\Omega} = N \tag{4}$$

where $\hat{\epsilon}\cdot\hat{\boldsymbol{R}}_j=\cos\Theta$ has been used. This yields the well-known form of the EXAFS equation for polycrystalline materials.

Equations (1–3) are strictly correct only for nearest-neighbor shells, since the single scattering approach does not usually hold for higher shells. In the transition metal dichalcogenides, however, the shortest double scattering

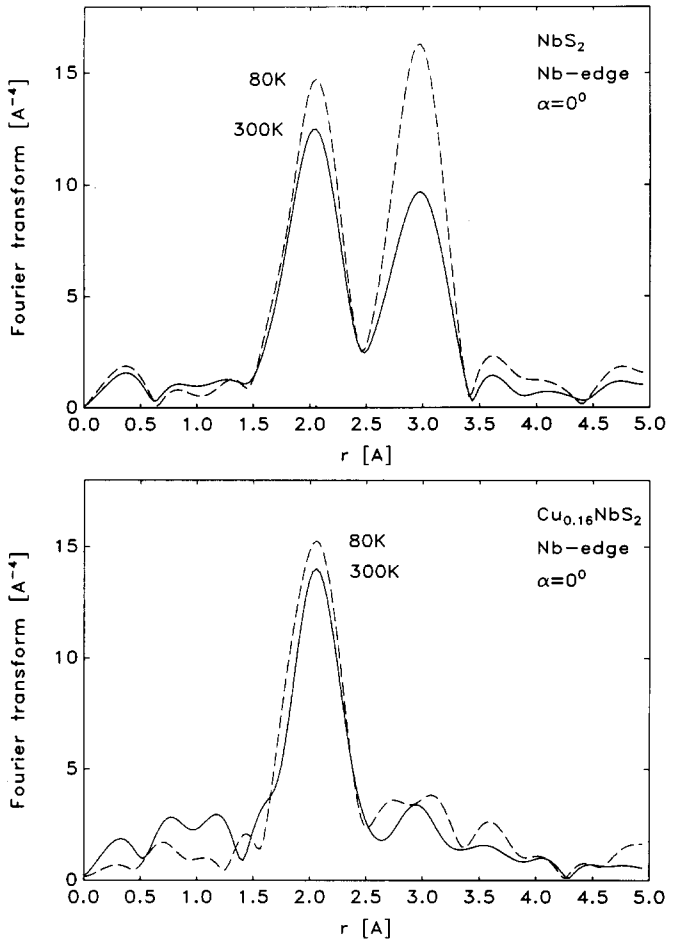

Fig. 4. Fourier forward transforms of Cu_xNbS_2 (Nb edge) as a function of temperature when the crystallographic c-axis is parallel to the X-ray beam ($\alpha=0$).

path is so much longer than the single scattering path to the next-nearest-neighbor and back that it is safe to neglect multiple scattering.

XANES data analysis of the Se edge is comparatively simple. The fit function consists of the sum of (i) a Victoreen function for the absorption contributions from electrons other than K electrons; (ii) one (two) lorentzian(s) for the pre-edge white line(s); (iii) one arctangent, shifted by 0.5 along the ordinate, and one lorentzian for adjusting the continuum states. Both the arctangent and the lorentzians are normalized to the K edge step height. The function is then convoluted with a gaussian to account for the monochromator resolution function. In order to obtain consistent results the fitting is carried out with the widths of the arctangent, the lorentzians and the gaussians set to constant values for each material.

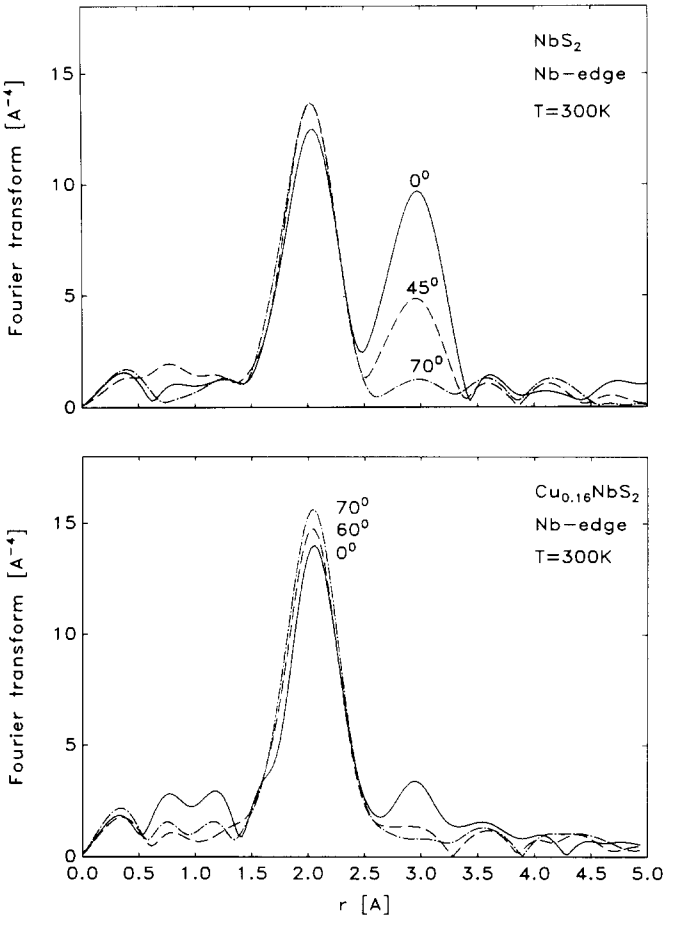

Fig. 5. Fourier forward transforms of Cu_xNbS_2 (Nb edge) as a function of the tilt angle at constant temperature.

3. EXAFS results and discussion

Inspection of the Fourier transforms (Figs. 3–5) allows a first qualitative interpretation of our results. It shows, first of all, a strong temperature dependence of the EXAFS signal. Also, with the reduction, or disappearance, of the next-nearest-neighbor shells, a marked difference is observed between the non-intercalated and the intercalated materials. The second shell is also very sensitive to a rotation of the crystal with respect to the X-ray beam.

The results of the quantitative EXAFS analysis are listed in Table 1. They include interatomic distances,

$$r = \langle r_{ij} \rangle \tag{5}$$

and second cumulants, or variances, of interatomic distances,

$$\sigma^2 = \langle r_{ij}^2 \rangle - \langle r_{ij} \rangle^2 \tag{6}$$

TABLE 1

EXAFS results for the nearest-neighbor and next-nearest-neighbor distances, r, and their second cumulants, or variances, σ^2. The error bars are about 0.01 Å for r and 1×10^{-3} Å^2 for σ^2

		NbS_2		$Cu_{0.16}NbS_2$	
		80 K	300 K	80 K	300 K
Nb–S distance	r (Å)	2.48	2.48	2.48	2.48
	σ^2 (10^{-3} Å^2)	1.5	2.9	1.5	2.0
Cu–S distance	r (Å)				2.44
	σ^2 (10^{-3} Å^2)				
Nb–Nb distance perpendicular to c-axis	r (Å)	3.32	3.32		
	σ^2 (10^{-3} Å^2)	4.0	6.7		
		$NbSe_2$		$Cu_{0.38}NbSe_2$	
		80 K	300 K	80 K	300 K
Nb–Se distance	r (Å)	2.59	2.59	2.59	2.60
	σ^2 (10^{-3} Å^2)	3.2	4.8	3.5	4.6
Se–Nb distance	r (Å)	2.59	2.59		
	σ^2 (10^{-3} Å^2)				
Se–Se distance perpendicular to c-axis	r (Å)	3.44	3.44	3.43	3.42
	σ^2 (10^{-3} Å^2)	4.7	9.5	9.2	15.3
Nb–Nb distance perpendicular to c-axis	r (Å)	3.44			
	σ^2 (10^{-3} Å^2)	3.1			

where the angle brackets indicate *thermal* and, if structural disorder exists, *structural* averaging of the interatomic distances between the absorbing atom i and atoms in the jth shell. The error bars are about 0.01 Å for r and 1×10^{-3} Å^2 for σ^2. Missing entries in Table 1 indicate our inability in some cases to obtain quantitative results with an accuracy of that size. This is mainly due to an insufficient separation of first and second shells in the Fourier forward transform, along with a small amplitude of the second shell.

The EXAFS results allow the following interpretation:

(i) The Nb–Nb and Se–Se distances of the non-intercalated samples, being identical to the lattice parameters a, compare very favorably with the literature values [1, 21] and our X-ray diffraction values [16], namely to within 0.01 Å, the value assigned to the error bar of r. The agreement is unusually good for an absolute distance determination of a next-nearest-neighbor shell from EXAFS.

(ii) Nb–S and Nb–Se distances are not affected by intercalation. The Se–Se in-plane distance in Cu_xNbSe_2 seems to shrink, which is probably due to our inability to separate clearly the Se–Se from the Se–Cu shells. Next-nearest-neighbor distances parallel to the c-axis could not be measured.

(iii) The observed Cu–S distance in $Cu_{0.16}NbS_2$ remains unchanged within our accuracy when the crystal is tilted, indicating equal distances for all Cu–S bonds.

(iv) The values of σ^2 of the non-intercalated systems at 80 K and 300 K are due to thermal motion; a structural disorder can be discarded. σ^2 increases with temperature, as expected, the increase being smaller for nearest-neighbor distances and larger for next-nearest-neighbor distances, because the correlation of the motion of two atoms decreases with increasing distance.

(v) The nearest-neighbor σ^2 value is not affected by intercalation ($+0.3$, -0.2×10^{-3} Å^2 for 80 and 300 K respectively); however, the next-nearest-neighbor Se–Se σ^2 value increases considerably upon intercalation of Cu into $NbSe_2$, the increase being 4.5 and 5.8×10^{-3} Å^2 for 80 K and 300 K respectively. Figure 3 shows how the next-nearest-neighbor peaks in the Fourier transforms are affected.

Our previous X-ray diffraction measurements [16] of the same $Cu_{0.38}NbSe_2$ sample indicate that intercalation of copper into the $NbSe_2$ crystal distorts the regularity of the trigonal prisms. This means, *e.g.* that the Nb–Se distance splits up into four different distances with a bond length variance, σ^2, of 0.1×10^{-3} Å^2. Correspondingly, the Se–Se distance splits up into three separate distances with $\sigma^2=5.8\times10^{-3}$ Å^2. These values yield an excellent confirmation of our EXAFS measurements or vice versa. It may therefore be concluded that intercalation is accompanied by a *structural* disordering of the host lattice.

(vi) The corresponding increase of the next-nearest-neighbor Nb–Nb σ^2 upon intercalation of Cu into NbS_2 and $NbSe_2$ could not be extracted quantitatively. However, as Fig. 4 shows for Cu_xNbS_2, the peak for the second Nb shell decreases even more dramatically than in Fig. 3. In Cu_xNbSe_2 (not shown) the second peak is already very small for $x=0$ and disappears completely when copper is intercalated. It indicates that the structural disorder is more pronounced between the Nb atoms than between the Se atoms in $Cu_{0.38}NbSe_2$.

(vii) The amplitudes of the first and second EXAFS shells depend markedly on the tilt angle, as shown in Fig. 5. With eqn. (2) and simple geometrical considerations the amplitude, A, of the first shell in Cu_xNbSe_2 can be calculated to be proportional to

$$A \alpha \sin^2\beta - (3\sin^2\beta - 2)\sin^2\alpha \tag{7}$$

where β is the angle between the c-axis and the direction of the Nb–Se bonds and $\alpha(=\pi/2-\Theta)$ is the angle between the c-axis and the direction of the X-ray beam (tilt angle). This is in qualitative agreement with the experiment. A similar calculation for the second shell is more difficult since three different Se–Se distances with different values for σ^2 enter the equation.

4. XANES results and discussion

We concentrate here on the Se edges measured in Cu_xNbSe_2. They exhibit a marked polarization dependence, as shown in Fig. 6. Figure 7

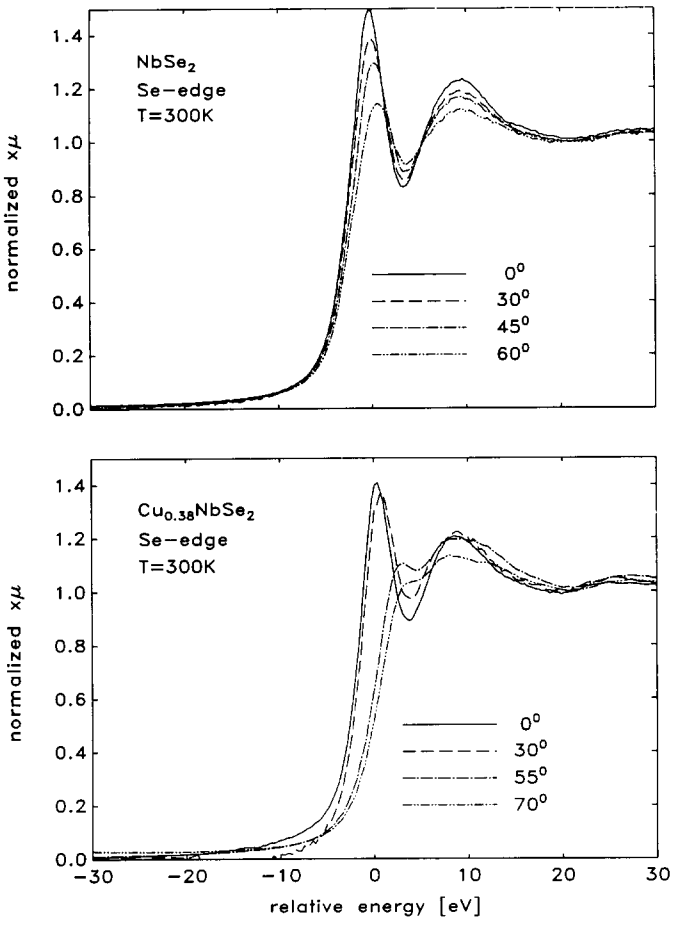

Fig. 6. X-ray absorption near-edge structures (XANES) of the Se edge of Cu_xNbSe_2 as a function of the tilt angle at constant temperature.

shows examples of the fits, as described above. Quantitative results are listed in Table 2. They include the positions relative to the Se reference white line maximum as well as the normalized heights of the pre-edge white line(s).

The XANES results allow the following interpretation:

(i) $NbSe_2$ has two pre-edge white lines, separated by about 2.5 eV, in accordance with the band structure calculations of Mattheiss [22] and Bullett [23]. A similar double-peaked structure has been observed in the sulfur *K*-edge spectrum of NbS_2, which is closely related to $NbSe_2$ in its electronic structure [11]. When Cu is intercalated into $NbSe_2$ the lower energy white line disappears. This is indicative of a charge transfer from the Cu atoms to the $NbSe_2$ host lattice reducing the number of empty electronic states of Se with z-symmetry.

(ii) When the crystal is tilted the relative height, and thus the number of empty states, of the lower energy white line increases, while the relative

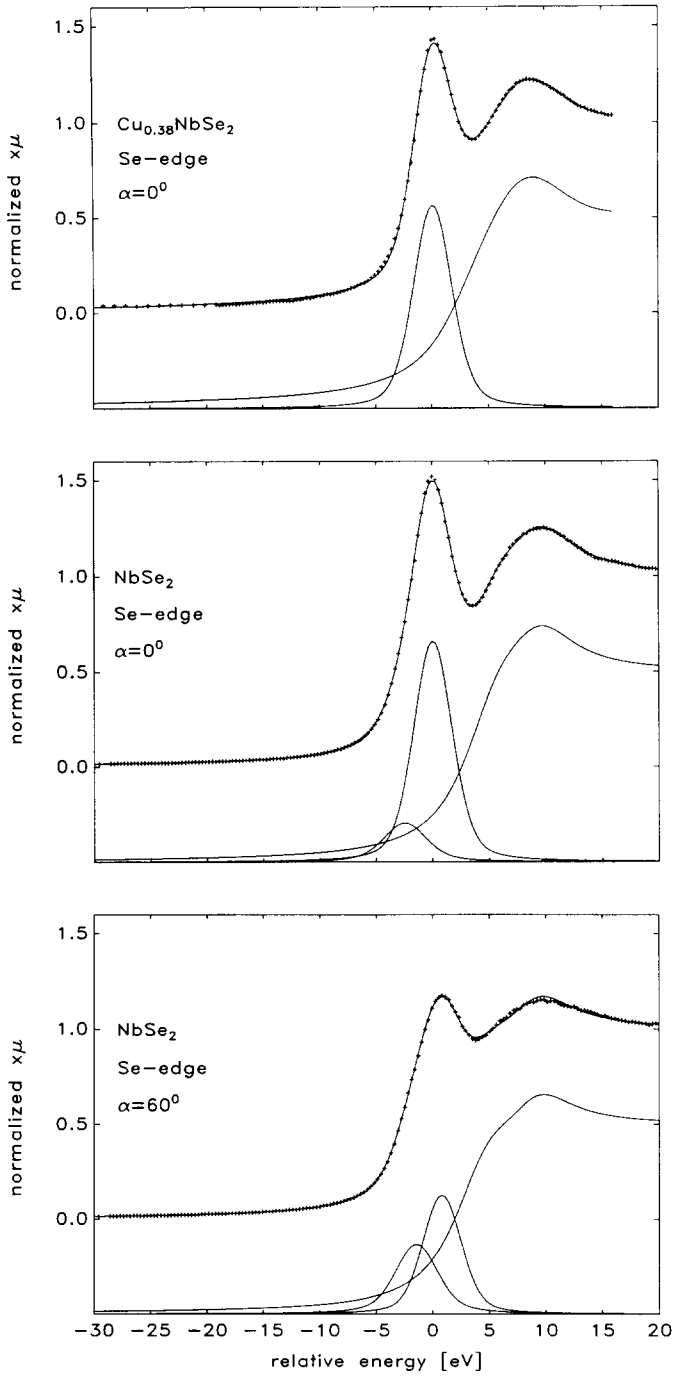

Fig. 7. Examples of least-square fits of the near-edge spectrum with the subspectra showing the pre-edge white line(s) and the continuum contribution consisting of a sum of an arctangent and a lorentzian.

TABLE 2

XANES results for the relative positions and relative heights (proportional to empty electronic states) of the first and second absorption lines in the Se edge of Cu_xNbSe_2

Tilt angle	1st line		2nd line	
	Relative position (eV)	Relative height	Relative position (eV)	Relative height
$NbSe_2$				
0°	−2.5	0.37	0.0	2.82
15°	−2.4	0.37	0.1	2.77
30°	−2.0	0.52	0.3	2.42
45°	−2.0	0.53	0.4	2.16
60°	−1.4	0.66	0.8	1.52
$Cu_{0.38}NbSe_2$				
0°	–	–	0.1	2.59
30°	–	–	0.7	2.26

height of the higher energy white line decreases. Recalling that absorption is at a maximum for states with a symmetry parallel to the direction of the X-ray polarization direction, $\hat{\epsilon}$, we conclude that the lower (higher) energy white line represents empty states with z- (x- and y-) symmetry.

(iii) Upon tilting the crystal, the position(s) of the white line(s) shift(s) to higher energies when compared with the Se reference white line absorption maximum. This is due to the fact that energy bands are angle sensitive.

(iv) Another indication for the above-mentioned charge transfer from the intercalated Cu atoms to the $NbSe_2$ host lattice is given by the change upon intercalation of the edge energy positions of the atoms involved. The Nb edge energy decreases by about 1 eV, while the Cu-edge energy (not shown) increases by 1–2 eV, when measured against the edge of metallic Cu. Similar such shifts are found for the Cu edge and the Nb edge in the NbS_2 system upon intercalation of Cu [13]. No noticeable shift is found at the Se edge.

5. Conclusion

(i) EXAFS can yield distances within 0.01 Å, in accordance with XRD, when high quality samples and data are used and analyzed with the presently available theoretical phases and amplitudes [18, 19].

(ii) The temperature dependence of σ^2 allows a distinction of temperature effects from disorder effects.

(iii) The edge contains valuable information about the electron structure and the intercalation induced changes. The analysis of the polarization dependence yields additional information about the symmetry of the orbitals involved.

Acknowledgment

This work was supported by the DFG (Sfb-337, TP B2) and the BMFT (Project No. 05 413AXI7/TP4).

References

1 R. M. A. Lieth and J. C. J. M. Terhell, in R. M. A. Lieth (ed.), *Preparation and Crystal Growth of Materials with Layered Structures*, D. Reidel, Dordrecht 1977, p. 141.
2 F. W. Boswell, A. Prodan and J. M. Corbett, *Phys. Status Solidi A, 35* (1976) 591.
3 B. E. Brown and D. J. Beerntsen, *Acta Crystallogr., 18* (1965) 31.
4 O. S. Rajora and A. E. Curzon, *Phys. Status Solidi A, 97* (1986) 65.
5 R. de Ridder, G. van Tendeloo, J. van Landuyt, D. van Dyck and S. Amelinckx, *Phys. Status Solidi A, 37* (1976) 591.
6 G. van Tendeloo, R. de Ridder, D. van Dyck, J. van Landuyt and S. Amelinckx, *Phys. Status Solidi A, 38* (1976) 185.
7 R. de Ridder, D. van Dyck, G. van Tendeloo, J. van Landuyt and S. Amelinckx, *Phys. Status Solidi A, 39* (1977) 383.
8 B. Sonntag and F. C. Brown, *Phys. Rev. B, 10* (1974) 2300.
9 A. J. Bourdillon, R. F. Pettifer and E. A. Marseglia, *Physica B, 99* (1980) 64.
10 B. M. Davies and F. C. Brown, *Phys. Rev. B, 25* (1982) 2997.
11 Y. Ohno, K. Hirama, S. Nakai, C. Sugiura and S. Okada, *Phys. Rev. B, 27* (1983) 3811.
12 Y. Ohno, K. Hirama, S. Nakai, C. Sugiura and S. Okada, *J. Phys. C, 16* (1983) 6695.
13 W. Thulke, R. Frahm, R. Haensel and P. Rabe, *Phys. Status Solidi A, 75* (1983) 501.
14 W. Thulke, R. Haensel and P. Rabe, *Phys. Status Solidi A, 78* (1983) 539.
15 P. R. Sarode, *Phys. Status Solidi A, 98* (1986) 391.
16 W. Paulus, G. A. Wiegers, A. Meetsma, S. van Smaalen and J. L. de Boer, *Phys. Status Solidi A, 114* (1989) 91.
17 J. Freund, R. Ingalls and E. D. Crozier, *Phys. Rev. B, 43* (1991) 9894.
18 J. J. Rehr, J. Mustre de Leon, S. I. Zabinsky and R. C. Albers, *J. Am. Chem. Soc., 113* (1991) 5136.
19 J. Mustre de Leon, J. J. Rehr, S. I. Zabinsky and R. C. Albers, *Phys. Rev. B, 44* (1991) 4146.
20 W. Krone, G. Wortmann and G. Kaindl, *Synth. Met., 29* (1989), F247.
21 A. A. Balchin, in F. Lévy (ed.), *Crystallography and Crystal Chemistry of Materials with Layered Structures*, D. Reidel, Dordrecht, 1976, p. 1.
22 L. F. Mattheiss, *Phys. Rev. B, 8* (1973) 3719.
23 D. W. Bullett, *J. Phys. C, 11* (1978) 4501.